# Multidimensional hydrodynamic plasma-wall model for collisional plasma discharges with and without magnetic-field effects

Haribalan Kumar and Subrata Roy[a)]
*Computational Plasma Dynamics Laboratory, Kettering University, Flint, Michigan 48504*

(Received 3 January 2005; accepted 2 August 2005; published online 15 September 2005)

A numerical model for two-species plasma involving electrons and ions at pressure of 0.1 torr is presented here. The plasma-wall problem is modeled using one- and two-dimensional hydrodynamic equations coupled with Poisson equation. The model utilizes a finite-element algorithm to overcome the stiffness of the resulting plasma-wall equations. The one-dimensional result gives insight into the discharge characteristics including net charge density, electric field, and temporal space-charge sheath evolution. In two dimensions, the plasma formation over a flat plate is investigated for three different cases. The numerical algorithm is first benchmarked with published literature for plasma formed between symmetric electrodes in nitrogen gas. The characteristics of plasma are then analyzed for an infinitesimally thin electrode under dc and rf potentials in the presence of applied magnetic field using argon as a working gas. The magnetic field distorts the streamwise distribution because of a large *y*-momentum $\boldsymbol{V}\times\boldsymbol{B}$ coupling. Finally, the shape effects of the insulator-conductor edge for an electrode with finite thickness have been compared using a 90° shoulder and a 45° chamfer. The 90° chamfer displays a stronger body force created due to plasma in the downward and forward directions. © *2005 American Institute of Physics*. [DOI: 10.1063/1.2044747]

## I. INTRODUCTION

Plasma discharge is commonplace in material processing and semiconductor industry, and is becoming popular in aerospace applications for plasma-based boundary layer flow control. A time accurate and geometry versatile numerical tool would prove useful in accurately calculating the discharge characteristics and its electrodynamic effects. The present effort is focused towards modeling and simulation of plasma discharge in the high-frequency, low-pressure regime.

The dynamics of sheath in one dimension in the low and intermediate pressure regimes have been studied in literature from numerical simulations.[1–5] Boeuf and Pitchford,[6] Dalvie *et al.*,[7] and Passchier and Godheer[8] simulated argon discharge for cylindrical geometry in two dimensions. Kim and Economou[9] investigated plasma formation over an inhomogeneous flat wall. Recent efforts have also considered the effect of external electromagnetic force on plasma-wall interaction.[10,11] In these simulations, fluid and/or particle-in-cell (PIC) formulation was used to model the system. Fluid equations are based on conservation laws derived from moments of Boltzmann equation while particle approaches such as PIC/direct simulation Monte Carlo (DSMC) involves plasma characterization by following millions of seed particles for each species. The choice of transport parameters under the continuum approximation is crucial in calculating the plasma characteristics accurately. The numerical advantage of using fluid descriptions is obvious for treating high-density plasma in which methods such as PIC become prohibitively expensive.

In spite of earlier attempts, the capability to simulate characteristics of a discharge in the presence of electric and magnetic fields remains limited. To contribute to this growing need, a hydrodynamic plasma model is presented in one and two dimensions. A high-fidelity finite-element procedure anchored in the multiscale ionized gas (MIG) flow code[12–14] is implemented to simulate the plasma using fluid description. The MIG code employs a self-consistent approach to model the near-wall physics of plasma gas interactions. In a self-consistent approach followed in many earlier works,[7,9,11–14] the space-charge effect is incorporated for the entire region. The sheath structure is investigated in the post-processing phase unlike the patching/matching techniques where bulk plasma forms a boundary condition to the sheath solution. Here, the plasma dynamics is investigated under steady and transient conditions over a flat plate for three different cases. The numerical algorithm is first benchmarked with published literature for nitrogen gas plasma formed between symmetric electrodes. Discharge characteristics of plasma for an infinitesimally thin electrode configuration are then analyzed under applied dc and rf potentials using argon as a working gas. Finally, the shape effect for an electrode with finite thickness is considered for a 90° shoulder and a 45° chamfer.

The paper is organized as follows. Section II describes the problem definitions, hydrodynamic equations, and fluid transport coefficients. Section III describes and interprets the results obtained for various discharge configurations. Section IV summarizes the conclusions.

## II. PROBLEM STATEMENT

The unsteady transport for electrons and ions is derived from fluid dynamics in the form of mass and momentum

[a)]Electronic mail: sroy@kettering.edu

 

conservation equations. The species momentum is modeled using the drift-diffusion approximation under isothermal condition that can be derived from hydrodynamic equation for electrons and ions neglecting inertial terms.[6,10,13] While one may include the inertia terms to get a slightly improved solution, at 0.1 torr pressure argon plasma sheath is collisional (see Ref. 15, p. 350) and the drift-diffusion approximation is reasonable and computationally efficient. Under the effect of collisions, the extent of charge separation is greater and the species velocity is greatly driven by electric body force ($qE$) as represented by this approximation. Electron temperature ($T_e$) is of the order of $\sim$11 600 K(1 eV) and ions are assumed cold at $\sim$300 K(0.026 eV). The continuity equation for ion and electron number densities is given by

$$\frac{\partial n_i}{\partial t} + \nabla \cdot (n_i \boldsymbol{V}_i) = \alpha |\Gamma_e| - r n_i n_e,$$

$$\frac{\partial n_e}{\partial t} + \nabla \cdot (n_e \boldsymbol{V}_e) = \alpha |\Gamma_e| - r n_i n_e, \tag{1}$$

$$|\Gamma_e| = \sqrt{(n_e V_e)_x^2 + (n_e V_e)_y^2},$$

where $n$ is the number density and $V$ is the species hydrodynamic velocity. As the sheath is collision dominated, electrons are not assumed to follow Maxwellian distribution. The electrochemical data provided here are for argon, which is the working gas for all cases except for a benchmark case for which nitrogen gas data have been used from Ref. 10. For a pressure of 0.1 torr, electron-ion recombination ($r$) is $\sim 2 \times 10^{-12}$ cm$^3$/s and has a negligible effect on mass balance.[6,16] The discharge is maintained using a Townsend ionization scheme. The ionization rate is expressed as a function of electron drift velocity and Townsend coefficients.[6,17,18] The Townsend coefficient $\alpha$ appearing in Eq. (1) is given by

$$\alpha = A p e^{-B/(|\boldsymbol{E}|/p)}, \tag{2}$$

where $A = 34$ cm$^{-1}$ torr$^{-1}$ and $B = 16$ V/(cm torr) are preexponential and exponential constants, respectively. $|\Gamma_e|$ is the effective electron flux and depends mainly on the electric field. The electronic and ionic fluxes in (1) are written as

$$n_i \boldsymbol{V}_i = n_i \mu_i (\boldsymbol{E} + \boldsymbol{V}_i \times \boldsymbol{B}_z) - D_i \nabla n_i, \tag{3}$$

$$n_e \boldsymbol{V}_e = -n_e \mu_e (\boldsymbol{E} + \boldsymbol{V}_e \times \boldsymbol{B}_z) - D_e \nabla n_e, \tag{4}$$

where the electrostatic field is given by $\boldsymbol{E} = -\nabla \varphi$. The Lorentz force term, $\boldsymbol{V} \times \boldsymbol{B}$that brings in the effect of magnetic field. The magnetic field is assumed to act along the $z$ direction, i.e., $\boldsymbol{B} = \{0, 0, B_z\}$. Since Eqs. (3) and (4) are of zeroth order, the bandwidth of the problem is considerably reduced by substitution into (1). This gives rise to a convection-diffusion-type equation, which apart from being more stable increases computational efficiency. After some algebraic manipulation, we end with the following equations:

$$\frac{\partial n_i}{\partial t} + \frac{\partial}{\partial x}\left\{ b_i\left( n_i \mu_i E_x - D_i \frac{\partial n_i}{\partial x} \right) + b_i \beta_i \left( n_i \mu_i E_y - D_i \frac{\partial n_i}{\partial y} \right) \right\} + \frac{\partial}{\partial y}\left\{ b_i\left( n_i \mu_i E_y - D_i \frac{\partial n_i}{\partial y} \right) - b_i \beta_i \left( n_i \mu_i E_x - D_i \frac{\partial n_i}{\partial x} \right) \right\} = \alpha |\Gamma_e|, \tag{5}$$

$$\frac{\partial n_e}{\partial t} + \frac{\partial}{\partial x}\left\{ b_e\left( -n_e \mu_e E_x - D_e \frac{\partial n_e}{\partial x} \right) - b_e \beta_e \left( -n_e \mu_e E_y - D_e \frac{\partial n_e}{\partial y} \right) \right\} + \frac{\partial}{\partial y}\left\{ b_e\left( -n_e \mu_e E_y - D_e \frac{\partial n_e}{\partial y} \right) + b_e \beta_e \left( -n_e \mu_e E_x - D_e \frac{\partial n_e}{\partial x} \right) \right\} = \alpha |\Gamma_e|, \tag{6}$$

where $b_{i,e} = 1/(1 + \beta_{i,e}^2)$ are functions of Hall parameters[10] $\beta_{i,e} = \mu_{i,e} B_z$.

In Eqs. (5) and (6), the effect of magnetic field on the discharge is theoretically brought into the system through introduction of an additional expression involving mobility. The convective term ($\nabla \cdot n\mu \boldsymbol{E}$) gets altered accordingly in the $x$ and $y$ directions. This affects the coupling between the electric field and number density resulting in transfer of momentum between axes. An appropriate choice of the magnitude and direction of the magnetic field **B** can accordingly increase or decrease the streamwise momentum through electrostatic forces. Modification in discharge characteristics is expected in a direction perpendicular to the significant axis of the problem.

The electron mobility in Eq. (6) is obtained from[17] $\mu_e = 3 \times 10^6$ cm$^2$ V$^{-1}$ s$^{-1}$, at $pd = 0.2$ torr cm. The electron diffusion coefficient, $D_e$, is calculated from the Einstein relation $D_e = kT_e/e\mu_e$. The ion diffusion coefficient is $D_i = 2 \times 10^2$ cm$^2$/s at 300 K. The ion mobility $\mu_i$ is expressed as a function of reduced field ($E/p$) (Refs. 6 and 17) as

$$p\mu_i = 10^3 [1 - 2.3 \times 10^{-3} E/p] \text{ cm}^2 \text{ V}^{-1} \text{ s}^{-1} \text{ torr} \quad \text{for } E/p \leqslant 60 \text{ V cm}^{-1} \text{ torr}^{-1},$$

$$p\mu_i = \frac{8.25 \times 10^3}{\sqrt{E/p}} \left[ 1 - \frac{86.5}{(E/p)^{1.5}} \right] \text{ cm}^2 \text{ V}^{-1} \text{ s}^{-1} \text{ torr} \quad \text{for } E/p > 60 \text{ V cm}^{-1} \text{ torr}^{-1}.$$

The relation between electrostatic field and charge separation is given by the Poisson equation

$$\varepsilon \nabla \cdot \mathbf{E} = -e(n_e - n_i). \tag{7}$$

For pressure of 0.1 torr in argon, as low as $\ll 1\%$ of secondary electrons are emitted back from the electrode. Hence, the electrodes are assumed to be fully absorbing. Secondary electron emission (SEE) can be neglected.

The system of equations (1)–(7) is normalized using the following normalization scheme: $\tau = \omega t$, $z_i = x_i/d$, $N_e = n_e/n_0$, $N_i = n_i/n_0$, $u_e = V_e/V_B$, $u_i = V_i/V_B$, and $\phi = e\varphi/kT_e$ where $V_B$

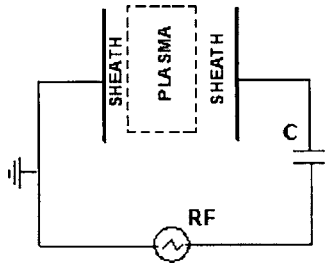


FIG. 1. Circuit schematic for one-dimensional model.

$=\sqrt{kT_e/m_i}$ is the Bohm velocity. For all the cases considered, $d=2$ cm, $\omega/2\pi=13.56$ MHz, and the reference density $n_0=2\times10^{15}$ m$^{-3}$.

## III. RESULTS AND DISCUSSIONS

The plasma-wall problem is solved using a finite-element formulation described in our previous works.[12–14] Briefly, the equation set (1)–(6) can be written generally as $L(\boldsymbol{q})=0$ where $\boldsymbol{q}$ is the vector containing $N_i$, $N_e$, and $\phi$. The discretized Galerkin weak statement (GWS) is written as

$$WS^h = S_e\left(\int_{\Omega_e}[\psi L(\boldsymbol{q})d\tau]\right)_e = 0. \tag{8}$$

$S_e$ is the nonoverlapping union of all elements $\Omega_e$ and $\psi$ is any permissible test function. The test function is chosen orthogonal to trial function in the GWS to ensure minimum solution error. The forward temporal evolution is evaluated using the fully implicit Euler time integration. The nonlinear Newton-Raphson scheme is used to solve the matrix using a LU decomposition solver for one-dimensional formulation and a generalized minimal residual solver to handle the sparseness of the resulting stiff matrix in two dimensions. The solution is assumed to have converged when the $L_2$ norm of all normalized solution variables and residuals is below a chosen convergence criterion ($\sim10^{-2}$). The system utilizes a subgrid embedded[13,19] (SGM) algorithm for computational stability and control of dispersion error. The SGM algorithm is incorporated into the dissipative flux terms based on the local cell velocity and is expected to ensure a nodewise monotone solution. A typical simulation takes about CPU time of 2.43 s for matrix assembly and 2.5 s at solver with an average of four to six iterations per time step. The solution for the applied time-varying input reaches a periodic state in the asymptote, which has been monitored through the evolution of discharge current and sheath thickness.

### A. One-dimensional discharge

The finite-element algorithm is employed to simulate the plasma for the schematic shown in Fig. 1. The applied potential (at electrode located at $x=2$) is varying as $\varphi_f=\varphi_{rms}\sin 2\pi ft$ with $\varphi_{rms}=100$ V and $f=13.56$ MHz. Also, $\varphi(0)=0$ and $\varphi(2)=\varphi_{rf}$. The sheath edge is identified by the modified Bohm[20] velocity as $V_B[1+c]^{-0.5}$ where $V_B$ is the Bohm velocity; the collision parameter $c=0.5\pi\lambda_{De}/\lambda_i$ is known for the Debye length $\lambda_{De}$ and the effective ion mean free path[15] $\lambda_i(\text{cm})\sim1/330p$ ($p$ is the gas pressure in torr) is assumed to be independent of velocity.

Figures 2–4 show the computed rf discharge characteristics for an applied frequency $\omega(\approx0.02\omega_{pe})\ll\omega_{pe}$. The distribution of electron gas in the gap between electrodes is periodic with applied frequency, as shown in Fig. 2(a). Near the electrode, an anode or cathode sheath is formed depending on the instantaneous wall potential. Figure 2(b) gives an approximate indication of sheath edge location at which space-charge separation becomes prominent as the ion and electron-density curves bifurcate. This also explains the direction and magnitude of electric field $E$ based on the space-charge sheath formed [Fig. 2(c)].

Ions, due to their higher inertia, respond weakly to the small fields in bulk plasma ($\omega>\omega_{pi}$). But, in the sheath where fields are high, the electrostatic forces are not negligible. Hence ions respond to the time-varying field and give rise at different time scales in bulk and sheath. Figure 2(d) shows the electron heating per elementary charge $[\boldsymbol{\Gamma}(\tau)\cdot\mathbf{E}(\tau)]$ profile. It is evident that electrons are periodically heated and cooled corresponding to the sheath oscillation and hence the electron energy increases or decreases accordingly. Sheath heating is a dominant phenomenon in radio-frequency-driven discharges. It should be noted here that the change in electron temperature due to this heating or cooling effect is not computed.

The variation of total current at the powered electrode for 3 cycles of applied potential is reported in Fig. 3(a). It should be noted that the displacement current and conduction (electron and ion) current magnitudes are comparable at the subject pressure of 0.1 torr. The peak of the total current is observed at every $(4n+1)\pi/2$. There is a minor secondary peak in Fig. 3(a) at the instant when the applied potential switches direction on the electrode.

The oscillation of sheath width $S_w$ is plotted in Fig. 3(b) using the Godyak-Sternberg relation. Based on curve fitting with an estimation error of $\sim4\%$, the sheath thickness is correlated as $S_w\approx0.04\pm0.03\sin\tau$. For the discharge at 0.1 torr, the simulation results predict the maximum sheath width $S_{w\text{-max}}\sim20\lambda_{De}$ which agrees with the available literature.[15,21] The sheath accounts for a nearly 80% potential drop for one rf cycle. The average normalized positive column length is 0.95 for the normalized electric-field strength of 3.2.

### B. Two-dimensional discharge

#### *1. Benchmarking with nitrogen gas*

As the lateral extent of a discharge becomes comparable to the transverse stretch in the presence of geometric or electrical inhomogeneities, the sheath becomes multidimensional and a one-dimensional model is not sufficient to capture the required features. Specifically, the interest to model the effect of magnetic field necessitates a higher dimensional consideration. First, the formulation is tested in two dimensions for

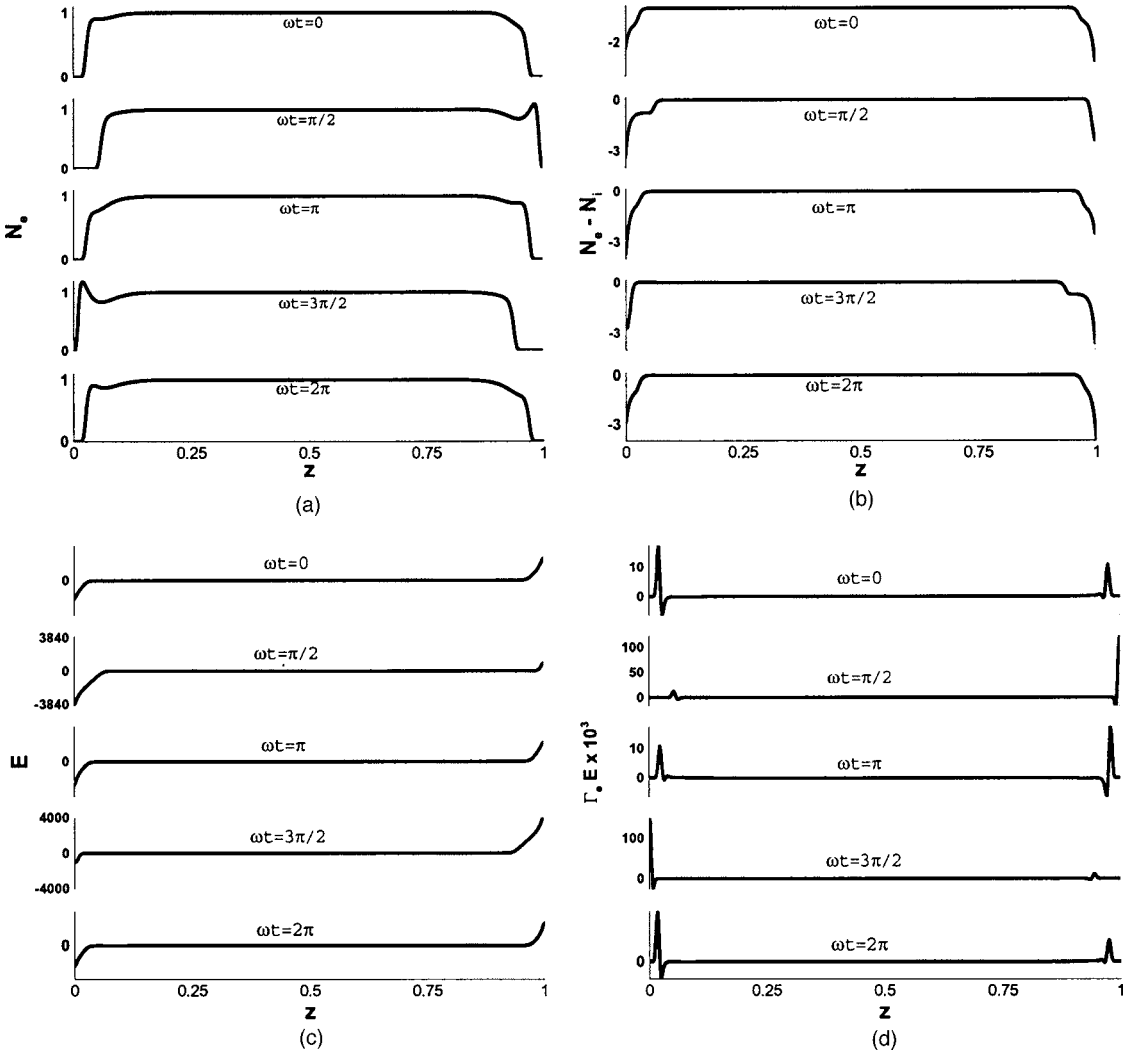


FIG. 2. Variation of normalized plasma parameters: (a) electron number density, (b) charge-density separation, (c) electric field, and (d) electron heating per elementary charge at various times of a single sinusoidal cycle.

plasma formed between two symmetric electrodes for a direct current glow discharge using nitrogen. The geometry and discharge conditions correspond to Surzhikov and Shang.[10] The computational grid consists of $25\times30$ biquadratic (9 node) finite elements. An electrode potential of 533 V is applied through an external circuit with resistance of 300 k$\Omega$ driven by an electromotive force of 2000 V. The model does not neglect diffusion in $x$ and $y$ directions for the entire domain including plasma and sheath.

The cathode is at $y=0$ while $y=2$ cm is the anode. Vanishing ion density is imposed at the anode while the electron density at the cathode is calculated from flux balance using a

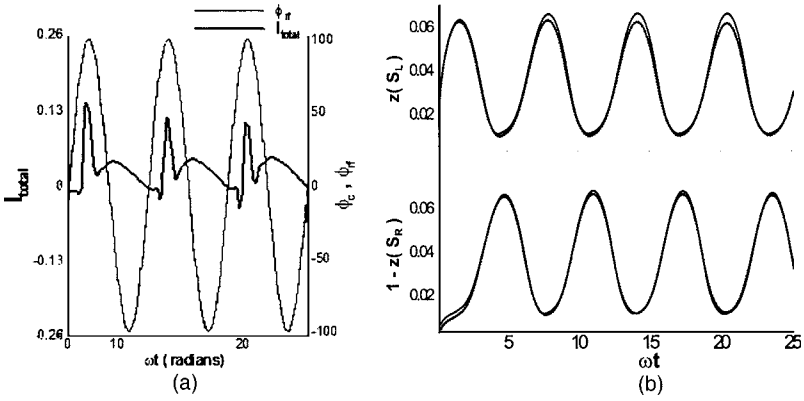


FIG. 3. (a) Temporal variation of total current and electrode potential, and (b) temporal evolution of left ($S_w=zL$) and right ($S_w=1\text{-}zR$) sheath widths.

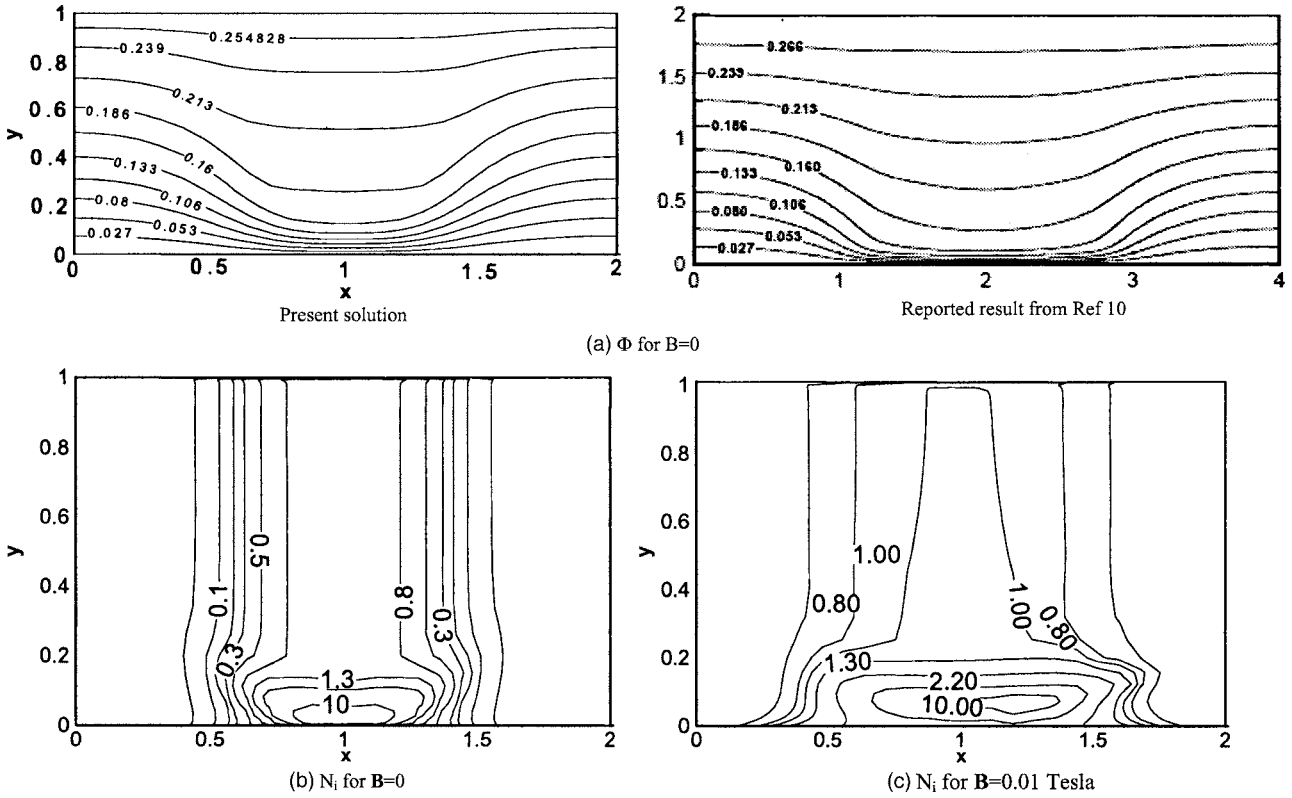


FIG. 4. (a) Electric potential contours, (b) ion density contours for $B=0$, and (c) ion density contours for $B=0.01$ T. All results shown here are for nitrogen gas at 5 torr.

secondary-emission coefficient of 0.1. The left and right boundaries of the computational domain are maintained at symmetry conditions. Electrons and ions are concentrated near the center of the geometry along the $x$ axis based on the initial condition calculated based on a preestimated cathode layer thickness and current column length.[10]

The simulation results for electric potential and ion density at pressure of 5 torr with and without the magnetic field are presented in Figs. 4(a)–4(c). The computed potential is compared with the results from Surzhikov and Shang[10] in Fig. 4(a) and is in good agreement. The potential lines are bent towards the cathode. This gives rise to high electric field (directed towards the electrode) driving electrons away forming a cathode sheath thickness ~7.5% of interelectrode gap. The ion density near the cathode rises to an order of magnitude higher than that near the center of the discharge channel and indicates a qualitative similarity.[10] When a magnetic field of 0.01 T is applied, the ion density peak gets shifted in the axial direction along the electrode surface [Fig. 4(c)]. A widening of discharge near the cathode is also observed. The direction of drift depends on the direction of the magnetic-field lines while the magnitude of shift of the isolines depends on the value of determinant of Eqs. (5) and (6).

### 2. Argon gas discharge

The formulation thus calibrated with reported result is then applied to model plasma of a pure argon gas discharge. The schematic model and the computational domain are shown in Fig. 5. The electrode is 1.78 cm long and the leading edge is located ~1.1 cm from the left boundary. The top surface is considered quasineutral. This assumption is valid

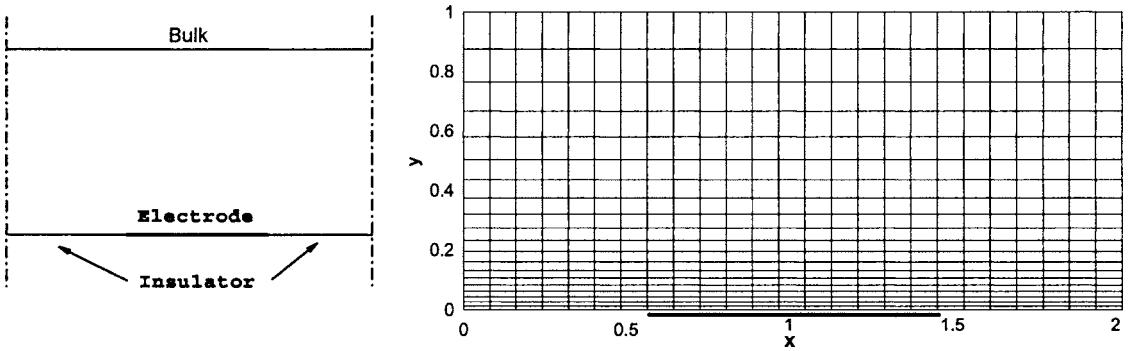


FIG. 5. Schematic of a perfectly flat electrode-insulator configuration and computational grid.

as the height of the domain chosen is much greater than the Debye length. A height of $\sim 200\lambda_{De}$ is chosen for the present case. The electrodes are assumed to have a negligible thickness compared to the dimensions of the model and are ignored for simplicity in this case.

The computational grid (see Fig. 5) consists of $25 \times 20$ biased biquadratic finite elements with the first node $\sim 0.01$ cm away from the wall. In the absence of magnetic field, the discharge may be treated as symmetric about $x=1$. Similar geometry has been treated recently in literature[9,11] for quiescent and fluctuating argon plasmas in the collisionless low-pressure regime. Apart from being a more realistic configuration this brings edge effects at the junction between the electrode and the insulator into consideration. The importance of understanding this discharge configuration proves useful in plasma-based flow control application that is being widely investigated as a means to alter near-wall boundary layer profile. A recent investigation studied the effect of plasma on neutral gas flow in an asymmetric configuration for dielectric barrier discharges (DBDs).[22] Hence this formulation provides a framework, which can be built upon to study high-pressure discharges and the effect of magnetic-field interaction in collision-dominated sheath.

Note that for this configuration in Fig. 5, there is a net flow of current into the metallic wall, while the current path is almost parallel to the dielectric surface. This gives rise to a near-wall inhomogeneity in the model, which might be compared to a mathematical discontinuity. This inherent feature introduces considerable numerical difficulty at the electrode-insulator edge. Due to the vast difference in potential across the insulator-conductor edge, maximum plasma generation is limited to this region which when not properly handled may affect numerical stability. As mentioned earlier, artificial stabilization techniques such as SGM with an upper bound on excess diffusion have been implemented to minimize dispersion error and ensure numerical stability of the solution.

For argon discharge, the systems of equations (1)–(4) and (7) are solved for dc and rf applied potentials using the following boundary conditions. The electron flux imposed at the electrode is based on the electron thermal velocity and directed towards the electrode. Electron flux normal to the electrode is considered as zero if drift velocity is away from the electrode. Boundary condition (at electrodes) for ions is imposed homogeneous Neumann ($\partial N_i/\partial n=0$). The normal current of charge carriers is nullified at insulator boundary. In the left and right boundaries, the slopes $\partial N_i/\partial x=0$, $\partial N_e/\partial x=0$, and $\partial \varphi/\partial x=0$ are enforced.

*a. dc discharge.* A steady-state discharge is first obtained without the magnetic field for an applied potential of $-50$ V on the exposed electrode. Figure 6(a) shows the isolines of computed electric potential. The symmetric nature of the contour in the absence of magnetic field about $x=1$ should be noted. The discharge is further modified by the application of a weak magnetic field $B_z=+5$ G. Figures 6(b)–6(d) compare the magnetic-field effect on the axial distribution of potential, electric-field, and charge-density differences close to the bottom plate after $10^{-9}$ s. Figures 6(e) and 6(f) plot the contour of electron number density for the two cases. Due to a large difference of potential between the top boundary and electrode, the variation of characteristic is noted along the $y$ axis. The magnetic field strongly affects the streamwise distribution because of high $y$-momentum transfer into the $x$ direction [as seen from Eqs. (5) and (6)]. The solid line shows the variation in the absence of magnetic field while the dotted line is for the imposed low magnetic-field intensity. The sharp change of characteristics (for example, spike-like pattern for net charge) near the electrode-insulator edge is expected. Most of the plasma formation is limited to this region. As shown in Fig. 6(b), the insulator is less cathodic ($\sim$25-V difference than cathode potential) and behaves like a pseudoanode collecting electrons. Corresponding to this pseudoelectrode, a sharp increase in electron density is observed near the highly depleted cathode sheath layer. In the presence of magnetic field, the potential lines (for example, near right electrode-insulator edge) are affected along the electrode surface as they are shifted from its initial position towards the right. This change is reflected in the charged species (through the Poisson equation) causing a variation in charge separation.

*b. rf discharge.* The steady-state discharge above was analyzed for fairly low magnetic-field intensity. With the gained theoretical understanding of electromagnetic interactions, a transient plasma discharge is simulated for a higher magnetic field of 20 G in the presence of an oscillating potential with a peak to peak of 100 V. In order to understand the variation of plasma characteristics in the presence of magnetic field, the solution is compared with a simulation without the magnetic field, all other conditions being the same.

The streamwise and transverse variations at different locations are shown in Figs. 7(a)–7(c). The results presented here are plotted along cuts in the vicinity of the edge for the negative half of the rf cycle. Figure 7(d) shows distribution of normalized plasma density in the domain. It was observed in the simulation that except for localized regions near the electrode-insulator edge, the magnetic field had a less pronounced effect on the transverse solution characteristic relative to streamwise components. This has been explained earlier from Eqs. (5) and (6). There are some significant observations that can be made. The solid line plots the streamwise and transverse variations in the presence of magnetic field against the dotted for no magnetic field. A $\sim$60% shift of potential is noted near the left insulator-conductor edge between the two cases. The asymmetry is more prominent in the case of 20-G field. Figure 7(b) shows electron number density close to the plate. In the presence of magnetic field, the electron drift velocities are altered and large electron accumulation (an order of magnitude higher than the discharge center) is observed near one of the insulator-conductor edges. Figure 7(c) shows the variation of axial electric field near the insulator-conductor interface. The 20-G field causes a 15 times increase in the near-wall field.

### C. Electrode shape effect

We have demonstrated that the presence of an insulator-conductor interface alters the nature of discharge and plays a

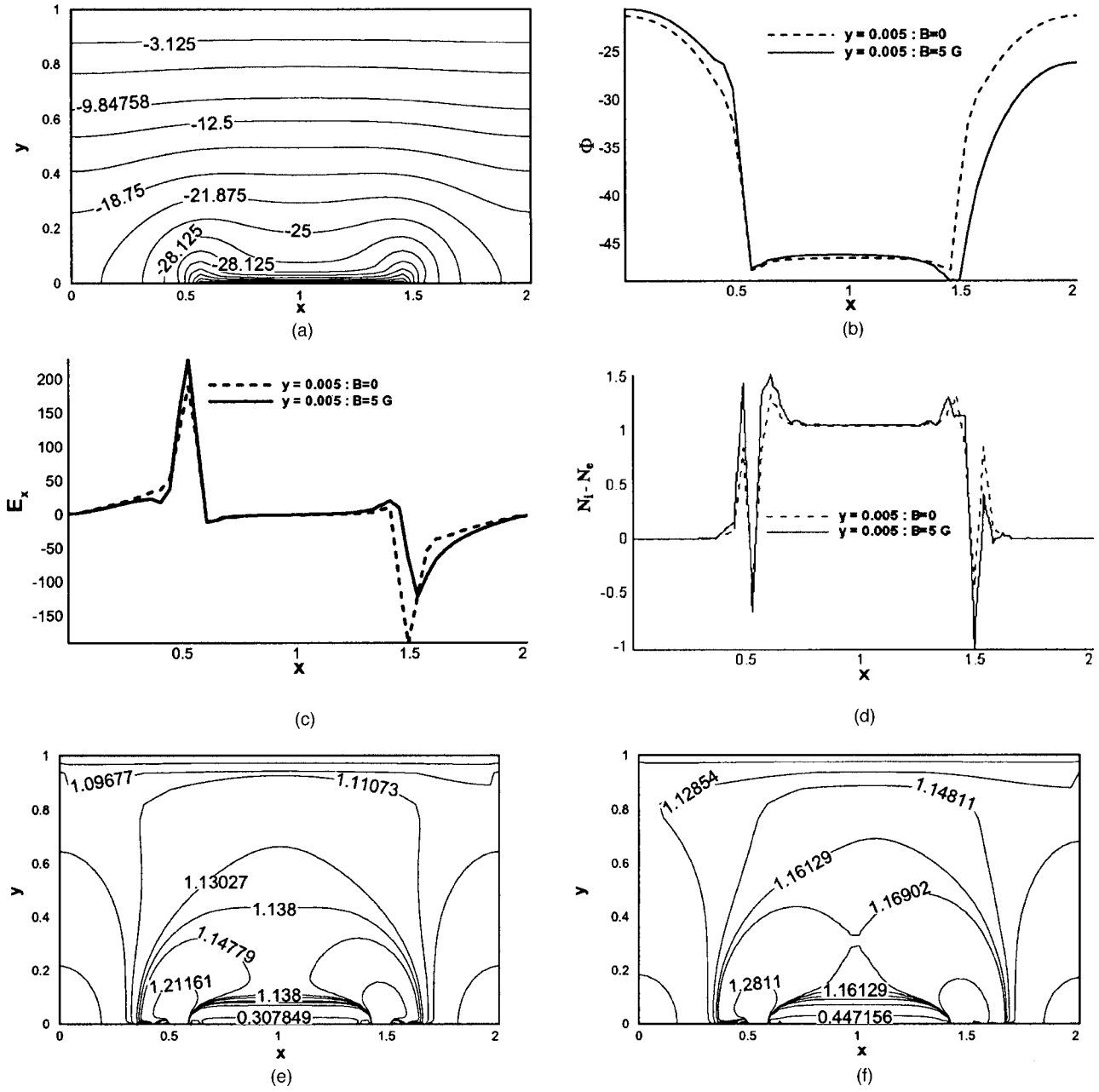


FIG. 6. dc discharge normalized results: [(a) and (b)] electric potential, (c) electric field, (d) net charge density variation, and [(e) and (f)] electron number density compared in the absence and presence of magnetic field. All results shown here are for argon at 0.1 torr.

significant role in altering electric forces due to plasma generation. The conductor in the previous case was assumed thin for simplicity in modeling. It has been shown recently that the shape of electrode plays a significant role in altering the nature of field lines and hence the $qE$ forces near the wall.[22,23] To have an insight into this shape effect, two configurations, shown in Figs. 8(a) and 8(b), are investigated in the present study. Figure 8(a) considers a sharp edge of electrode with a 90° shoulder while Fig. 8(b) considers an edge with a 45° shoulder. The case of rounded edge [Fig. 8(c)] may be visualized as an intermediate case between the 90° and 45° shoulder configurations.

This study is limited to a steady state in the absence of magnetic field for simplicity. The leading edge of an electrode with 0.2-mm thickness is located at 1.5 cm from the left boundary. The computational grid consists of $45 \times 45$ biquadratic finite elements in both cases. The discharge conditions are the same as before, namely, 0.1-torr argon plasma with an electrode potential of −50 V.

Figures 9(a)–9(f) show the computed profiles for the above-mentioned cases. The region near the edge has been zoomed for clarity. From a common understanding, the 90° edge creates a sharp geometrical discontinuity resulting in an abrupt change in the radius of curvature across the edge as compared to the bevel. Hence, the spatial variation of electric field gets considerably modified altering the electrodynamic properties of the discharge between the two shapes. The electric-field lines for a given change in the potential are shown in Figs. 9(a)–9(d) and the effects are felt within few Debye lengths (~0.1 cm) into the plasma.

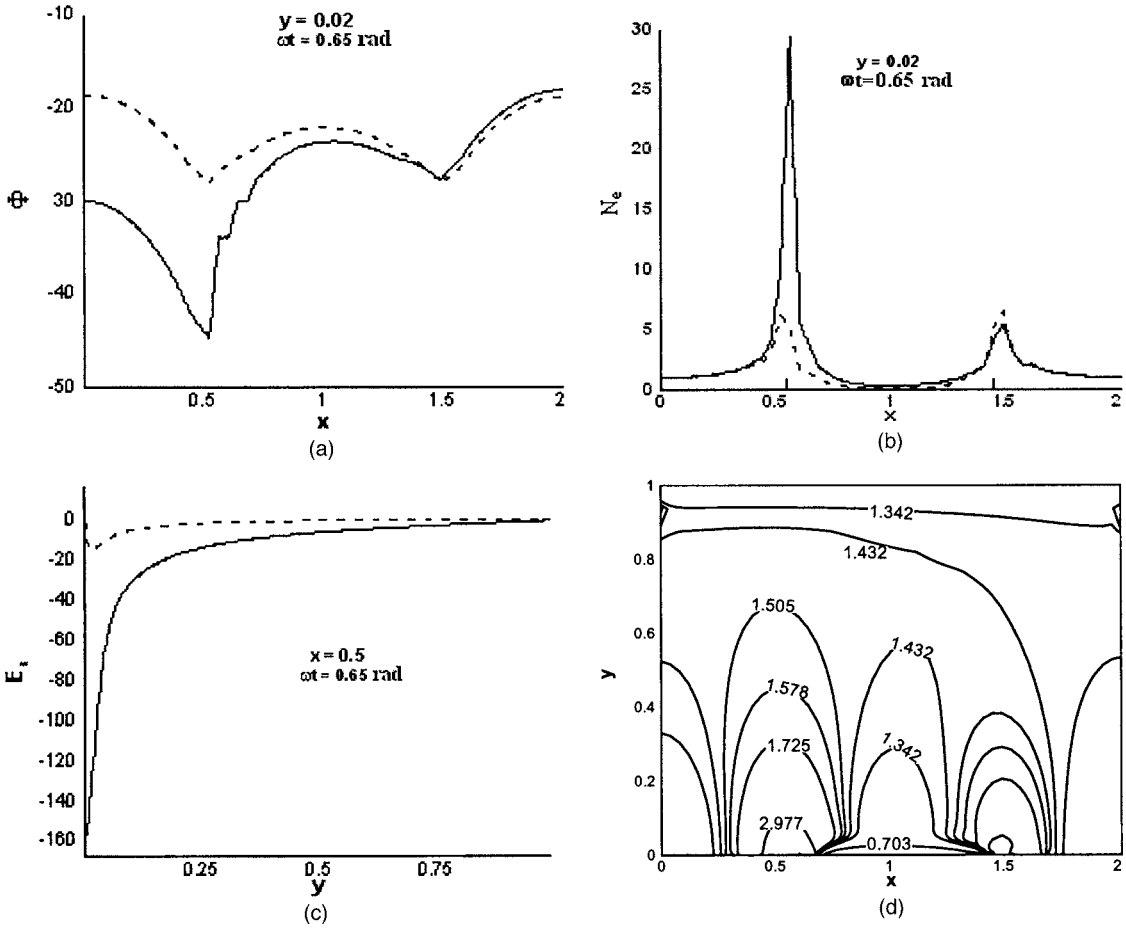


FIG. 7. Normalized rf discharge characteristics: (a) streamwise potential along $y=0.02$, (b) electron number density contour along $y=0.02$, (c) axial electric field along $x=0.5$, and (d) electron-density distribution. The solid line shows the variation in the presence of magnetic field of 20 G. The dotted line is for $B=0$. All results shown here are for argon at 0.1 torr.

Figures 9(e) and 9(f) plot the force vector for the two shapes expressed as a product of space-charge difference $(N_i\text{-}N_e)$ and electrostatic field ($E_x$ or $E_y$). In both cases, a strong electrostatic force in the positive $x$ and negative $y$ directions is noted close to the wall. The presence of cathode gives rise to a strong transverse field (with electric-field lines ending at the cathode perpendicular to it) downstream of the edge. The direction of the electric force vector [given by $\tan^{-1}(F_y/F_x)$] near the wall was predicted between 225° and 260° oriented mostly in the third quadrant. This is indicative of an effective forward-downward force created by the plasma across the edge. As compared to the beveled edge, the sharp 90° corner with the smallest radius of curvature shows an ~22% increase in $E_x$ and 15% increase in $E_y$ near the edge resulting in about the same percentage increase induced force components.

## IV. CONCLUSIONS

An argon gas discharge under applied rf potential between two electrodes has been modeled from first principles using a self-consistent coupled system of two-fluid and single Poisson equations. The dynamics of ions and electrons have been reported for an applied rf frequency $\omega < \omega_{pe}$ and 0.1 torr pressure. The collisional nature of the problem, varying time scales for charged species in the bulk plasma and sheath, and the use of an interpolation polynomial to simulate the plasma-sheath transition that has abrupt changes in gradients add to the complexity of the problem. The oscillation of the sheath edge has been correlated as a sinusoidal wave. The sheath is of few Debye lengths and accounts for a nearly 80% potential drop for one rf cycle.

The formulation was tested in two dimensions for

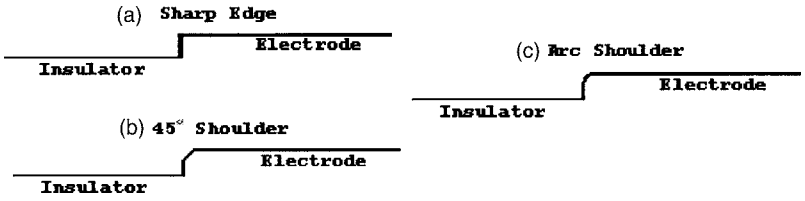


FIG. 8. Electrode-insulator edge types. (a) Sharp edge, (b) 45° shoulder, and (c) arc-shaped shoulder.

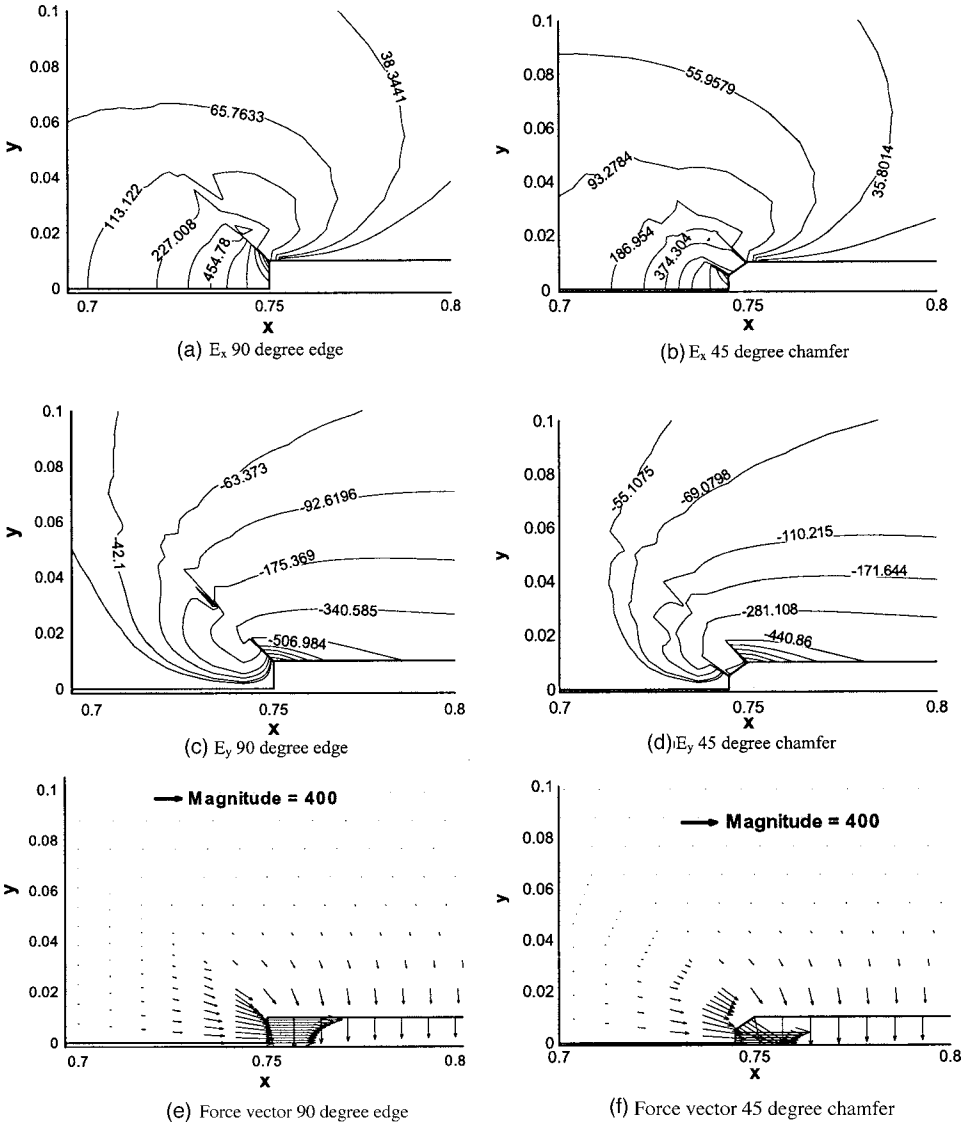


FIG. 9. Normalized axial electric field ($E_x$) and transverse electric field ($E_y$) contours and force vectors for a 90° shoulder and 45° shoulder. (a) $E_x$ 90° edge, (b) $E_x$ 45° chamfer, (c) $E_y$ 90° edge, (d) $E_y$ 45° chamfer, (e) force vector 90° edge, (f) force vector 45° chamfer.

plasma formed between two symmetric electrodes for a direct current glow discharge using nitrogen. The results match well with published literature. A steady-state discharge is simulated for argon in an electrode-insulator configuration. The magnetic field has been shown to strongly affect the streamwise distribution caused by the $\boldsymbol{V}\times\boldsymbol{B}$ coupling between $x$ and $y$ axes. Simulation results for a transient discharge evolution in the presence of time-varying rf potential have been investigated. The present analyses have served to highlight the importance of understanding two-dimensional gas discharge nature and the effect of time-varying potential and an external magnetic field on it. More rigorous treatment will follow in a future work. Finally, the shape effect in insulator-conductor configuration on near-wall dynamics is compared using a 90° shoulder and 45° chamfer. The maximum axial force is about 22% higher for a 90° shoulder while the force vector across the edge indicates a net downward and forward force generated.

The potential of combined electric and magnetic fields as a productive means in altering near-wall plasma forces has been realized here. The results presented are expected to help interpret the plasma formation in the presence of electromagnetic interaction on the discharge structure for higher pressures. As a future effort, we also intend to correlate the plasma characteristics for varying magnetic-field intensities.

[1] P. A. Miller and M. E. Riley, J. Appl. Phys. **82**, 3689 (1997).
[2] D. Bose, T. R. Govindan, and M. Meyyappan, J. Appl. Phys. **87**, 7176 (2000).
[3] Y. Zhang, J. Liu, Y. Liu, and X. Wang, Phys. Plasmas **11**, 3840 (2004).
[4] T. E. Nitschke and D. B. Graves, J. Appl. Phys. **76**, 5646 (1994).
[5] H. Kumar and S. Roy, *43rd AIAA Aerospace Sciences Meeting and Exhibit*, Reno, NV, 2005 (AIAA, Washington, DC, 2005), AIAA-2005-0948.
[6] J. P. Boeuf and L. C. Pitchford, Phys. Rev. E **51**, 1376 (1995).
[7] M. Dalvie, M. Surendra, and G. S. Selwyn, Appl. Phys. Lett. **62**, 3207 (1993).
[8] J. D. P. Passchier and W. J. Goedheer, J. Appl. Phys. **74**, 3744 (1993).
[9] D. Kim and D. J. Economou, J. Appl. Phys. **94**, 2852 (2003).
[10] S. T. Surzhikov and J. S. Shang, J. Comput. Phys. **199**, 437 (2004).
[11] L.-J. Hou, Y.-N. Wang, and Z. L. Miskovic, Phys. Plasmas **11**, 4456 (2004).
[12] S. Roy and D. Gaitonde, J. Appl. Phys. **96**, 2476 (2004).
[13] S. Roy, B. P. Pandey, J. Poggie, and D. Gaitonde, Phys. Plasmas **10**, 2578 (2003).
[14] S. Roy and B. P. Pandey, Phys. Plasmas **9**, 4052 (2002).
[15] M. Lieberman and A. J. Lichtenberg, *Principles of Plasma Discharges and Material Processing* (Wiley, New York, 1994).
[16] A. D. Richards, B. E. Thompson, and H. H. Sawin, Appl. Phys. Lett. **50**,

492 (1987).
[17]L. Ward, J. Appl. Phys. **33**, 2789 (1962).
[18]I. D. Kaganovich, L. D. Tsendin, and N. A. Yatsenko, Tech. Phys. **39**, 1215 (1994).
[19]S. Roy and A. J. Baker, Numer. Heat Transfer, Part B **33**, 5 (1998).
[20]V. A. Godyak and N. Sternberg, Phys. Rev. A **42**, 2299 (1990).
[21]Y. P. Raizer, M. N. Shneider, and N. A. Yatsenko, *Radio-Frequency Discharges* (CRC, London, 1995).
[22]S. Roy, Appl. Phys. Lett. **86**, 101502 (2005).
[23]C. L. Enloe, T. E. McLaughlin, R. D. VanDyken, K. D. Kachner, E. J. Jumper, T. C. Corke, M. Post, and O. Haddad, AIAA J. **42**, 595 (2004).